Earth and Planetary Science Letters 603 (2023) 117970

Contents lists available at ScienceDirect

Earth and Planetary Science Letters

journal homepage: www.elsevier.com/locate/epsl

Serpentinite fluids and slab-melting in the Aleutian arc: Evidence from molybdenum isotopes and boron systematics

Ekaterina Rojas-Kolomiets [a,*], Owen Jensen [a], Michael Bizimis [a], Gene Yogodzinski [a], Lukáš Ackerman [b,c]

[a] School of Earth, Ocean and Environment, Department of Geology, University of South Carolina, 701 Sumter St., EWSC617, Columbia, SC 29208, USA
[b] Institute of Geology of the Czech Academy of Sciences, Rozvojová 269, 165 00, Prague 6, Czech Republic
[c] Czech Geological Survey, Geologická 6, 165 00, Prague 5, Czech Republic

ARTICLE INFO

Article history:
Received 6 July 2022
Received in revised form 11 December 2022
Accepted 16 December 2022
Available online xxxx
Editor: R. Hickey-Vargas

Keywords:
molybdenum isotopes
boron
subduction zones
arc magmas
serpentinite fluids
sediments

ABSTRACT

Mo isotope compositions have been increasingly used as a source tracer in magmatic systems. Here, we investigate the relative role of subducting oceanic crust, fluid-rich sources (e.g., serpentinite, altered oceanic crust – AOC), subducted sediments and upper mantle in the chemical composition of Aleutian arc magmas with Mo and B systematics. We present elemental and Mo isotope compositions ($\delta^{98/95}$Mo) and B concentrations on Aleutian lavas (n = 59), from Okmok Volcano in the east to the westernmost seamount Piip, showing absence of Mo isotope fractionation during magmatic differentiation. Additionally, we report Mo isotope systematics for serpentinized peridotites from the South-West Indian Ridge (SWIR) (n = 6), AOC (n = 2) and Pacific sediments (DSDP 183, ODP 886) (n = 5) outboard the Aleutian arc. Molybdenum isotope composition and B enrichment (e.g., B/Ce) patterns display a step-function increase along the arc, with low, MORB-like, $\delta^{98/95}$Mo and low B/Ce values in the western section of the arc (B/Ce = 0.15–1.07; $\delta^{98/95}$Mo = −0.38 to +0.01‰), that abruptly increase in the central-eastern volcanoes Korovin, Seguam and Yunaska (B/Ce = 1.20–2.60; $\delta^{98/95}$Mo = +0.03 to +0.30‰) near the intersection of the Amlia Fracture Zone (AFZ) with the trench, but decrease again farther east at Okmok (B/Ce = 0.76 and $\delta^{98/95}$Mo = −0.12‰ on average). These data patterns are interpreted to reflect an along-arc changing source in the Aleutian magmas. AOC and Pacific sediments have predominantly low $\delta^{98/95}$Mo (−0.47 to −0.32 and +0.17 to −1.9‰, respectively), while serpentinites have extremely high $\delta^{98/95}$Mo (up to +1.09‰) and high B/Ce (~22000). Based on the low $\delta^{98/95}$Mo in sediments and AOC, and lack of correlation between along-arc $\delta^{98/95}$Mo and radiogenic sediment tracers, subducted sediments and AOC do not exert first-order controls on the observed Mo isotope compositions. Rather, low, MORB-like, $\delta^{98/95}$Mo but high Mo enrichments (e.g., Mo/Ce) in the western samples are consistent with slab melting under rutile-bearing eclogitic facies with near absent Mo isotope fractionation from the slab to the arc sources. In turn, the abrupt increase of $\delta^{98/95}$Mo and B/Ce in lavas near the AFZ are best explained by a serpentinite endmember (likely dehydration fluids) at the AFZ that is not evident elsewhere along the arc. Results from this study provide evidence for serpentinites as an additional heavy Mo isotope signature component in subduction zones and demonstrate that high $\delta^{98/95}$Mo coupled with B enrichments are a useful proxy for tracing serpentinite fluids in subduction zones.

1. Introduction

Phanerozoic subduction zones produce up to 95% of Earth's continental mass (Rudnick, 1995; Plank and Langmuir, 1998) and contribute to the chemical evolution of the planet through recycling of volatiles and related rock-and-mineral materials from the upper crust back into the mantle. The compositions of volcanic products reflect the relative contributions and nature of the mantle wedge, subducted sediments, oceanic crust, and slab-derived dehydration fluids (e.g., Gill, 1981; Spandler and Pirard, 2013). Of these sources, fluids are particularly important because they enhance melting and control the budgets of many of the fluid-mobile elements. However, the nature and amounts of slab-derived fluids and other source components vary significantly by location due to

* Corresponding author.
E-mail address: erojaskolomiets@seoe.sc.edu (E. Rojas-Kolomiets).

https://doi.org/10.1016/j.epsl.2022.117970
0012-821X/

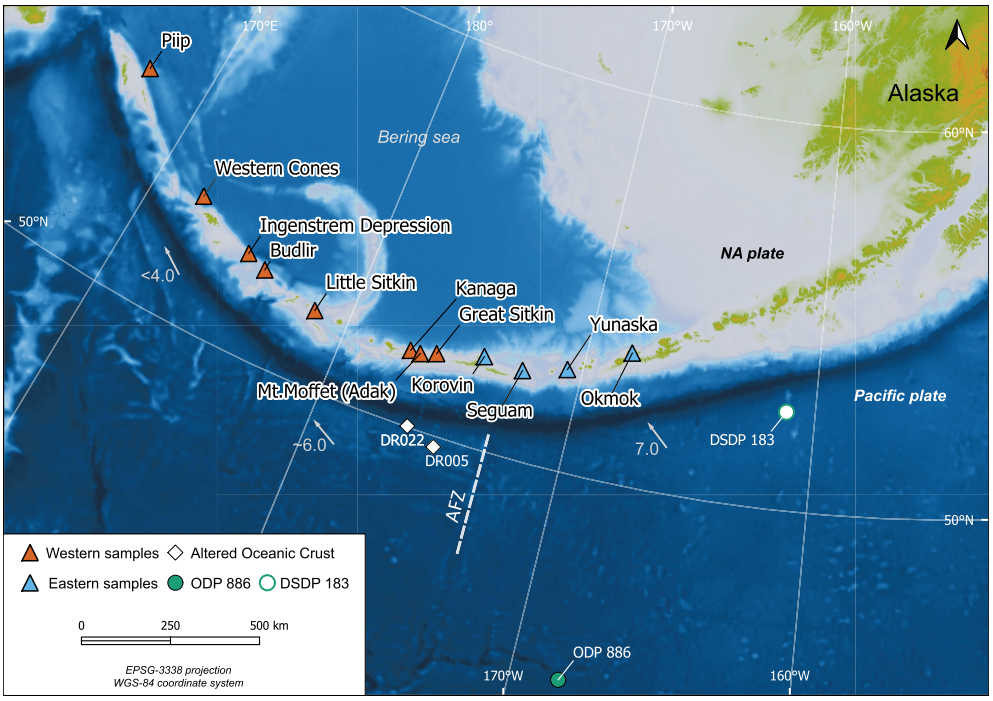

Fig. 1. Location of Aleutian volcanoes, AOC and sediments (DSDP 183, ODP 886) analyzed here. Orange and light blue triangles represent western and eastern lavas, respectively. Light gray arrows show direction and convergence velocity of the subducting Pacific plate (in cm/year) under the North American (NA) plate (Kelemen et al., 2003). Transparent white dashed line represents location of the Amlia Fracture Zone (AFZ). North arrow in the upper left corner represents the grid north. (For interpretation of the colors in the figure(s), the reader is referred to the web version of this article.)

differences in subduction zone inputs, slab geometry, and thermal regime.

The Aleutian arc offers an ideal natural laboratory to identify the relative contributions of the different endmembers involved in arc volcanism. The incoming Pacific plate changes from fast (7 cm/yr, Fig. 1), nearly orthogonal convergence in the east, where subducted sediments increasingly contribute to the arc magmatism (Kelemen et al., 2003; Yogodzinski et al., 2010), to a slow (<4 cm/yr, Fig. 1) and oblique subduction in the westernmost arc, where slab melting under eclogitic facies is evident in the volcanic products (Yogodzinski et al., 2015, 2017). These changes in subduction regime contribute to a coupled change in the rate of sediment subduction which peaks at ~173°W (~95 m^3/m/yr), where the Amlia Fracture Zone (AFZ) enters the trench (Fig. 1). The AFZ is a 1 km-high escarpment on the Pacific plate (Scholl et al., 1982) that entered the trench near Yunaska Island ~5 Ma ago and has since been transported ~300 km westward to its current position between Korovin and Seguam (Fig. 1; Singer et al., 2007). The high rate of sedimentary input at the AFZ is produced by the east-facing escarpment which inhibits the westward sediment transport down the axis of the trench from the Gulf of Alaska (Scholl et al., 1982). The overall effect is that both sediment thickness and sediment flux are doubled on the east side of the AFZ (3.7–4 km, 20 m^3/m/yr, respectively) compared to the west (2.0–2.5 km, 90 m^3/m/yr) (Kelemen et al., 2003; Scholl et al., 1982). Along-arc delivery of sediment to the trench west of the AFZ is primarily a function of subduction rates which decline progressively to the west (Kelemen et al., 2003). Key effects of these changes in subduction regime are expressed in the compositions of Aleutian volcanic rocks which display patterns for Pb, Sr, Nd, and Hf isotopes that are consistent with declining inputs of subducted sediment from east to west along the arc (Kelemen et al., 2003; Yogodzinski et al., 2010, 2015).

Although the contributions of sediments, subducting oceanic crust and upper mantle have been explored systematically for the full length of the arc (e.g., Kelemen et al., 2003; Yogodzinski et al., 2017), the fluid sources are less well constrained (e.g., Singer et al., 2007). Here, we focus on the relative contributions of subducting fluid-rich sources (e.g., serpentinite, altered oceanic crust – AOC), subducted sediment and upper mantle to the source of Aleutian-arc magmas using Mo and B systematics, both characterized as fluid-mobile elements in subduction systems (Bali et al., 2012; Ryan and Chauvel, 2014). We present Mo isotopic and concentration data, and B concentrations for fifty-nine well-characterized volcanic rocks from twelve volcanic centers spanning ~1800 km along the arc, from Okmok Volcano in the east to Piip Seamount in the west (Fig. 1). Analyzed samples cover the full range of Aleutian-arc compositions, including the basalts from Seguam Island with Pb isotopes nearly as radiogenic as Aleutian trench sediments and the western Aleutian Mg-andesites and dacites with radiogenic isotopes similar to northeast Pacific MORB. To help constrain the compositions of Aleutian subduction inputs, we also report Mo isotope data for samples of marine sediments, serpentinized peridotites, and Pacific AOC. In this study, we discuss three key areas: (1) the effects of igneous differentiation and amphibole fractionation on Mo isotopes, (2) the dominant source of Mo enrichment over Ce in Aleutian volcanic rocks, and (3) the effects on Mo isotope systematics of fracture zone subduction in samples from volcanos that straddle the AFZ location.

2. Samples and analytical methods

2.1. Data and samples

We report Mo elemental and isotope compositions (as $\delta^{98/95}$ Mo relative to the NIST SRM 3134) and new B concentration data

on basalts, basaltic andesites, andesites and dacites from the emergent Aleutian volcanoes Buldir, Little Sitkin, Mt. Moffet (Adak Island), Kanaga, Great Sitkin, Korovin (Atka Island), Seguam, Yunaska, Okmok (Unmak Island) and from submarine volcanoes Piip, Ingenstrem Depression, and the Western Cones (Arndt, 2011; Jicha et al., 2004; Singer et al., 2007; Yogodzinski et al., 2010, 2015, 2017) (Fig. 1). Our data set includes the first B concentration data for Korovin and for all western samples from Buldir to Piip. To identify possible effects on Mo and B from igneous differentiation at Korovin and Buldir, we also present in-situ trace element concentrations for phenocrysts and matrix measured by LA–ICP–MS.

To facilitate the along-arc description of the data, we refer to sample locations as the western and eastern lavas or sample groups. Eastern samples are from Korovin, Seguam, Yunaska, and Okmok while western samples are from Buldir, Little Sitkin, Kanaga, Moffet and Great Sitkin (Fig. 1). The western samples also include the westernmost Mg-andesites and Mg-dacites produced by seafloor volcanism at the Ingenstrem Depression, Western Cones, and Piip Seamount. These samples are primitive with Mg-numbers >0.60 (Mg# = molar Mg/Mg+Fe) and include several with fractionated (adakitic) trace element patterns that require a role for residual garnet in the source and cannot be related by igneous differentiation to other compositions in the dataset.

Additional sampling at Korovin and Buldir over a wide range of SiO_2 (50–64 wt%) allows us to investigate the effects of fractional crystallization and other forms of igneous differentiation on Mo isotopes in two distinct volcanic centers. Measurements by SIMS on olivine-hosted melt inclusions indicate that pre-eruptive H_2O contents at Korovin were 4–5 wt%, which is somewhat higher than ~3.7 wt% inferred from the THI (Tholeiitic Index) value of 0.79 (Zimmer et al., 2010). Buldir is significantly more calc-alkaline (Fig. S1) with a THI of 0.69 which – applying the method of Zimmer et al. (2010) – translates to an estimated H_2O content of ~5.9 wt%. The lower THI and implied higher H_2O content is qualitatively consistent with experimental constraints indicating that amphibole is a near-liquidus phase at Buldir (Waters et al., 2021). This is in turn consistent with the presence of amphibole as the main ferromagnesian phenocryst in Buldir andesites and dacites (Figs. S1-S2) and with presence of amphibole even in mafic Buldir lavas with only 52 wt% SiO_2 (Kay and Kay, 1985). These mineralogical characteristics at Buldir contrast sharply with those observed at Korovin where the mineral assemblage is dominated by plagioclase and pyroxene and remains anhydrous (amphibole-free) throughout the series from 50 to 64 wt% SiO_2.

Finally, to constrain the compositions of Aleutian subduction inputs, we also report Mo isotope and Mo concentrations data for marine sediments (n= 5), Pacific altered oceanic crust (AOC) (n= 2), and serpentinized peridotite (n= 6). Sediment samples are from drill cores at ODP 886C and DSDP 183 sites, located on the Pacific Plate south of the eastern Aleutian trench (Fig. 1). The AOC samples are dredged Pacific MORB collected by the RV Sonne (SO249) from locations immediately south of the central Aleutian trench (Fig. 1, Werner et al., 2016). Serpentinized peridotite samples are abyssal peridotites from Southwest Indian ridge (SWIR) (Frisby et al., 2016a, 2016b) included to provide general constraints on the compositions of serpentinized peridotite that may be present in subducting Pacific lithosphere. All Mo isotope and concentration data, as well as B concentrations and other compositional data of the analyzed samples are provided in the Supplemental Materials (Table S1).

2.2. Analytical methods

Molybdenum chemical isolation and mass spectrometry analyses were undertaken at the Center for Elemental Mass Spectrometry (CEMS), University of South Carolina and selected samples (denoted with "CZ" in Table S1) at the joint laboratory of the Institute of Geology of the Czech Academy of Sciences/Czech Geological Survey (IG CAS). Molybdenum isotope compositions were determined combining the double-spike (Willbold et al., 2016) and the NIST SRM 3134 standard bracketing method (CEMS) or sole double-spike technique (IG CAS; Gaspers et al., 2020). Powdered rock samples (~200 mg) were spiked with a ^{97}Mo–^{100}Mo double-spike at optimum levels (Rudge et al., 2009) and digested using a 3:1 mixture HF–HNO_3 (Teflon-distilled) following multiple re-dissolutions with 6M HCl. Chemical separation of Mo follows the method in Willbold et al. (2016), using fresh, pre-cleaned resin (Eichrom AG 1x8 100-200). Molybdenum isotope ratios in both labs were determined on a Thermo Scientific™ Neptune MC–ICP–MS. At CEMS, the raw data was reduced following Siebert et al. (2001) scheme on MATLAB while IG CAS utilized an algebraic approach with an exponential term and cascade iteration. Molybdenum concentrations were calculated using the isotope dilution equation. The precision and accuracy were evaluated by repeated $\delta^{98/95}$Mo and Mo concentration analyses of separately dissolved BHVO-2, JB-2 and AGV-2 reference materials, with results well-consistent with previous determinations (Table S1). Analytical uncertainties are represented using the most conservative reproducibility (multiple digestions) of ±0.05‰ (2 s.d.) of the rock standards AGV-2, BHVO-2, and JB-2. However, sample reproducibility was generally better than ±0.05‰ (Table S1). Mo concentrations for unknown sample replicate varied more than AGV-2, which we attribute to sample heterogeneity. Full procedural blanks, mostly originated from the resin, averaged 0.5 ng of Mo, and are considered negligible due to the high Mo contents analyzed. We note that the Eichrom AG 1x8 100-200 mesh resin has a significantly lower Mo blank than the equivalent Bio-Rad resin.

Boron concentrations were determined at CEMS by isotope dilution ICP–MS using a method modified after (Menard et al., 2013). Rock powders were spiked with NBS-952 ^{10}B spike. After digestion with HF, samples were diluted directly without drying and analyzed on a Thermo-Scientific Element2 ICP–MS. Mass bias was corrected by bracketing unknowns with the NBS-951 boron isotope standard using $^{11}B/^{10}B$= 4.04362. External precision of the protocol is 2–3% based on repeated measurements of AGV-1 and BCR-2.

Trace element concentrations of rock matrix and phenocrysts for BULD 0546 (Table S2) were determined using a Photon Machines Excimer 193 nm laser system coupled to an Element2 high-resolution ICP–MS at CEMS following the methods of Frisby et al. (2016a). With "matrix" here we mean area of the thin section absent of phenocrysts, although microcrystalline assemblages (<5 µm) may be present, but much smaller than the ~ 60 to 100 µm beam used for the analyses. See Supplemental Materials for more details on Mo, B and LA–ICP–MS methods.

3. Results

3.1. Molybdenum isotope systematics

The Aleutian arc lavas display a wide range of Mo isotope compositions (−0.38 to +0.30‰. Figs. 2–3). Western Aleutian samples have low $\delta^{98/95}$Mo (−0.38 to +0.01‰) with an average of −0.16‰ identical within error to estimates of the primitive mantle (−0.21 to −0.16‰; Burkhardt et al., 2014; Liang et al., 2017), depleted mantle (−0.20‰; McCoy-West et al., 2019) and MORB (−0.27 to −0.04‰, excluding the two heavy $\delta^{98/95}$Mo outliers from Bezard et al., 2016; Chen et al., 2022; Hin et al., 2022). In contrast, $\delta^{98/95}$Mo values increase abruptly in the eastern lavas at Korovin, Seguam and Yunaska ($\delta^{98/95}$Mo= +0.03 to +0.30‰, +0.13‰ on average), with values higher than continental crust estimates ($\delta^{98/95}$Mo = +0.05 to +0.15‰, Liang et al., 2017; Voegelin et al., 2014), before decreasing again in the easternmost volcano of

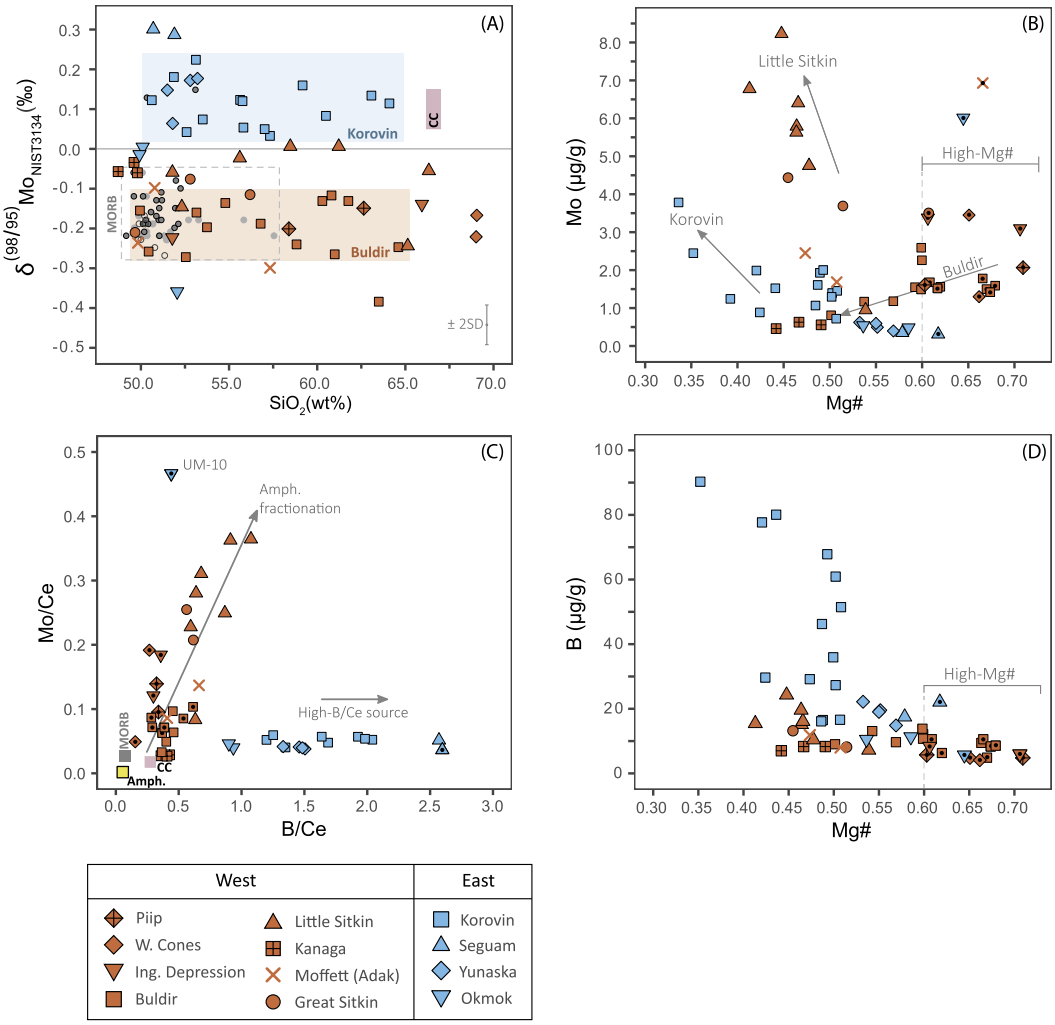

Fig. 2. Mo isotope systematics and B concentration for Aleutian arc lavas. **(A)** $\delta^{98/95}$Mo vs. SiO_2 (wt%). Shaded rectangles represent the general distribution of Korovin and Buldir lavas. Gray dashed rectangle shows the general distribution of MORB estimates (excluding the two high $\delta^{98/95}$Mo MORB samples) (Bezard et al., 2016, dark gray circles), (Chen et al., 2022, light gray circles), (Hin et al., 2022, hollowed gray circles). **(B)** Mo concentrations vs. Mg#. High-Mg# dacites correspond to westernmost samples with Mg# >0.6. Gray arrow shows general tendency of Korovin, Little Sitkin and Buldir plot patterns. **(C)** Mo/Ce vs. B/Ce. Gray, and pink bars represent average MORB and Continental Crust (CC), respectively. MORB B concentrations from Marschall et al. (2017) and Ce from Gale et al. (2013). Mo isotope data for CC from Liang et al. (2017) and Voegelin et al. (2014). Mo and Ce concentrations from Rudnick and Gao (2003). Aleutian Ce and SiO_2 data from Singer et al. (2007); Arndt (2011); Yogodzinski et al. (2010, 2015). Data points with black circles represent primitive samples (Mg#>0.6). Gray bar represents analytical uncertainty (±2SD) of ±0.05‰ (see main text, Section 2.2).

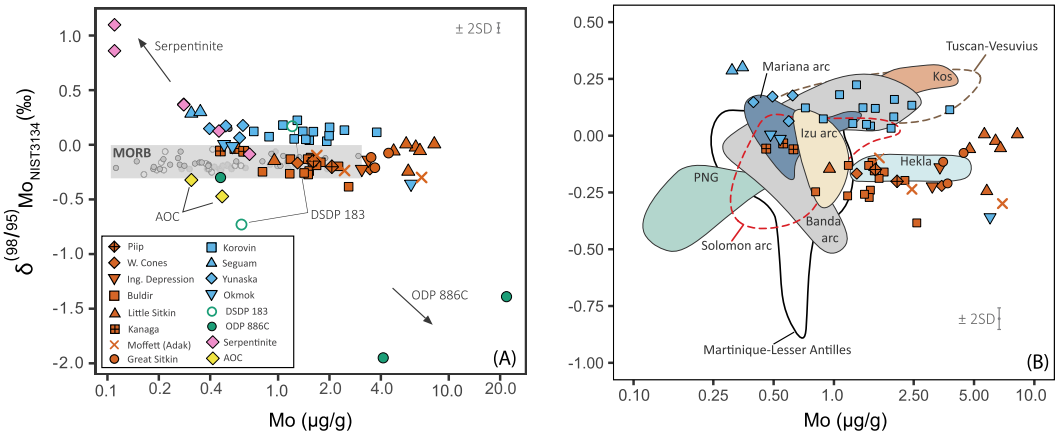

Fig. 3. Mo isotopes vs. Mo concentrations for Aleutian lavas and volcanic rocks globally. **(A)** $\delta^{98/95}$Mo vs. Mo concentrations for Aleutian lavas (see legend in the lower left corner), Pacific sediments (Hollow green circles for DSDP 183 and filled green circles from ODP 886C), serpentinized peridotites (magenta diamonds) and AOC (yellow diamonds). Light gray bray represents general distribution of MORB data (Bezard et al., 2016; Chen et al., 2022; Hin et al., 2022). **(B)** $\delta^{98/95}$Mo vs. Mo concentrations for Aleutian lavas, Hekla (Yang et al., 2015), Mariana arc (Freymuth et al., 2015), Banda arc (Wille et al., 2018), Kos (Voegelin et al., 2014), Tuscan-Vesuvius (Casalini et al., 2019), Solomon and PNG (König et al., 2016), Lesser Antilles (Freymuth et al., 2016), Martinique (Gaschnig et al., 2017) and Izu arc (Villalobos-Orchard et al., 2020). Gray bar represents analytical uncertainty (±2SD) of ±0.05‰.

our study – Okmok ($\delta^{98/95}$Mo= −0.36 to 0.00‰, −0.12±0.20‰ on average) (Fig. 4C).

Molybdenum concentrations in the Aleutian volcanic rocks are largely variable (0.31 to 8.23 µg/g,) (Table S1, Fig. 3). In general, eastern, and western samples overlap in their Mo concentrations (Fig. 3A). However, eastern samples extend to lower Mo (0.31–3.78 µg/g, excluding UM10 sample from Okmok with 6.01 µg/g Mo) compared to the western lavas (0.46–8.23 µg/g). Molybdenum concentrations increase with decreasing Mg# (used here as a proxy for magmatic differentiation), in Little Sitkin and Korovin (up to ∼8 and ∼4 µg/g for the lowest Mg#, respectively, Fig. 2B), while the remaining volcanoes show invariant Mo concentrations with Mg#. Western Aleutian lavas display high Mo enrichments (e.g., Mo/Ce, based on the similar partitioning of Mo and Ce during mantle melting), with Mo/Ce =0.03–0.36, up to one order of magnitude higher than MORB (0.01–0.06; Bezard et al., 2016), while eastern samples display lower and nearly constant Mo/Ce ratios (0.04–0.06, excluding UM10) closer to MORB and continental crust (∼0.02, Rudnick and Gao, 2003) (Fig. 2C).

Arc lavas from the two different calc-alkaline Korovin and Buldir differentiation sequences have distinct Mo isotope signatures. The $\delta^{98/95}$Mo values in Buldir are low (−0.38 to −0.12‰, on average −0.21 ± 0.08‰), but high in Korovin (+0.03 to +0.22‰, on average +0.11 ± 0.06‰) (Table S1). In either volcano, the $\delta^{98/95}$Mo values do not correlate with the wide range of SiO_2 (∼50 to 65 wt%) or Mo concentrations (Korovin= 0.72–3.78 µg/g and Buldir= 0.81–2.59 µg/g) (Figs. 2A and 3).

Pacific sediments from DSDP 183 and ODP 886C sites exhibit a wide range of $\delta^{98/95}$Mo (−1.95 to +0.17‰) and Mo concentrations (0.46–21.8 µg/g) (Fig. 3A). Diatom ooze and Mn-Fe nodules/concretions from ODP 886C (Rea et al., 1993) (886C-7H and 886C-3H) have extremely low $\delta^{98/95}$Mo (−1.39 and −1.95‰, respectively), but high Mo concentrations (4.13–21.8 µg/g) compared to pelagic clays from the same site (886C-1H with $\delta^{98/95}$Mo = −0.30‰, Mo= 0.46 µg/g). In contrast, sediments from DSDP 183 have variable $\delta^{98/95}$Mo (−0.73 to +0.17‰) for the same lithological unit (Unit D, a turbiditic sequence of clays with sporadic silts and sands, Creager et al., 1973) and a narrow range of Mo concentrations (0.61 to 1.21 µg/g). Sample 183-38R-2-68-70 with relatively high $\delta^{98/95}$Mo (+0.17‰) belongs to the lower terrigenous horizon of Unit D, characterized by a gray-greenish clay with interbedded silts and sands and laminated fissile shales that become more abundant at the bottom of Unit D (∼400 m) (Creager et al., 1973). In turn, sample 83-27H-3-36-38 with low $\delta^{98/95}$Mo (−0.73‰) is characterized by a clay sediment composition from the upper pelagic horizon (∼250 m) within the same unit (Creager et al., 1973).

Serpentinized abyssal peridotites have high $\delta^{98/95}$Mo (−0.08 to +1.09‰) and Mo concentrations (0.11 to 0.68 µg/g) far higher than primitive mantle (∼0.02 ng/g; McDonough and Sun, 1995), but in the range of MORB (0.09–2.94 Mo µg/g; Bezard et al., 2016; Chen et al., 2022; Hin et al., 2022) (Fig. 2A, 3A). The AOC samples exhibit a narrow range of Mo concentrations (0.31–0.47 µg/g) similar to MORB. However, their $\delta^{98/95}$Mo values (−0.47 to −0.32‰) are lower than found in MORB and similar to the AOC samples from Tonga (Ahmad et al., 2021) but contrast with the high-$\delta^{98/95}$Mo AOC from the Marianas (Freymuth et al., 2015).

3.2. Boron concentrations

Aleutian lavas show a wide range of B concentrations (4.09–90 µg/g, Table S1). Western lavas have low B concentrations (4.09–24.3 µg/g) that are nearly constant across the Mg# range (∼0.4–0.7), while eastern lavas display high B concentrations at Korovin (16.6–90 µg/g) but low at Seguam, Yunaska and Okmok (5.7–22.2 µg/g) that increase with decreasing Mg# (Fig. 2D). B/Ce is low and relatively constant among western Aleutian lavas (0.15–1.07, 0.52 average), but increases in Korovin, Seguam, and Yunaska (1.20–2.60, 1.72 average), and decreases at Okmok (0.44–0.93, 0.76 on average) (Fig. 4D). The SWIR serpentinized peridotites have high B concentrations (70–89 µg/g) and high B/Ce ratios (∼640–22000), approximately nine orders of magnitude higher than the primitive mantle (∼0.0002; McDonough and Sun, 1995) (Table S1).

3.3. Amphibole trace element concentrations

Amphiboles in BULD 0546 andesite have variable and low Mo (0.03–0.19 µg/g) and B (0.9–2.8 µg/g), but high Ce concentrations (23–44 µg/g). The rock matrix has Mo concentrations (0.25–0.30 µg/g) that are ∼3 times higher than found in amphibole (on average) and B concentrations (10.7–15.5 µg/g) ∼8 times higher than that of average amphibole, but Ce concentrations (21–70 µg/g) like amphibole phenocrysts. Orthopyroxene and plagioclase phenocrysts have very low Mo (0.01 µg/g) and B concentrations (∼0.8 µg/g) (Table S2, Figs. 2C and S3).

4. Discussion

4.1. Source versus differentiation effects: constraints from $\delta^{98/95}$Mo and Mo–B

Variability in $\delta^{98/95}$Mo values for Aleutian volcanic rocks (−0.38 to +0.30‰, Figs. 2A and 3) is larger than the difference between MORB and continental crust, and encompasses nearly the entire $\delta^{98/95}$Mo range observed in island arcs globally (Fig. 3B – Ahmad et al., 2021; Casalini et al., 2019; Freymuth et al., 2015, 2016; Gaschnig et al., 2017; König et al., 2016; Villalobos-Orchard et al., 2020; Voegelin et al., 2014). Two key aspects of the dataset are the low MORB-like $\delta^{98/95}$Mo in the western samples and the sudden increase in $\delta^{98/95}$Mo in the vicinity of the AFZ (Fig. 4C). This abrupt change in $\delta^{98/95}$Mo suggests that the main control over Mo isotopes lies in the source of Aleutian magmatism which changes along the arc. This inference is consistent with the lack of correlation between $\delta^{98/95}$Mo and SiO_2 at Buldir and Korovin (Fig. 2A), suggesting that, with or without amphibole, fractional crystallization, and related forms of calc-alkaline differentiation at Korovin and Buldir do not produce significant fractionation of Mo isotopes. This is in turn consistent with absence of Mo isotope fractionation across a wide spectrum of compositions in volcanic systems globally (e.g., Hekla; Yang et al., 2015, Tonga; Ahmad et al., 2021, Vesuvius-Tuscan; Casalini et al., 2019, Izu; Villalobos-Orchard et al., 2020).

Variable Mo and B concentrations and relative enrichments provide important insights into the behavior of these elements in subduction magmatic systems. Increases in B and Mo concentrations at Korovin with decreasing Mg# (Figs. 2B-D) and major oxides (Fig. S4) are consistent with incompatible behavior for both elements. In the western-group samples, however, the effects of differentiation on Mo and B are less clear. At Little Sitkin and Great Sitkin, Mo concentrations are variable but overall increase with decreasing Mg# over a narrow range of relatively evolved compositions (Mg# <0.55 – Fig. 2B). At Buldir, we observe the opposite, with Mo concentrations that decrease with decreasing Mg# (∼0.65 to 0.44, Fig. 2B). Molybdenum concentrations are moderate-to-high (∼1–3 µg/g) in the high Mg-andesites and dacites which are uniformly primitive (Mg#>0.60 – Fig. 2B) indicating that incompatible element abundances have been little-affected by igneous differentiation. Finally, all remaining western samples have B abundances that are low and nearly invariant relative to Mg# and MgO (Figs. 2D and S4).

Some aspects of the variable Mo and B concentrations described above can be linked to effects of amphibole fractionation during igneous differentiation. This is supported by obtained laser ablation trace element data for amphibole phenocrysts from a Buldir andesite (Table S2, Fig. S3). These data show systematically lower Mo and B concentrations in amphiboles compared to the matrix indicating that Mo and B are relatively incompatible in amphibole. In contrast, Ce is more strongly partitioned into the amphibole (Table S2), with an apparent amphibole/matrix partition coefficient close to 1, consistent with the experimentally determined partitioning of light REEs in andesitic magmas (Nandedkar et al., 2016). Therefore, fractionation of an amphibole-bearing mineral assemblage must lead to an increase in Mo/Ce as observed in evolved western samples (Mg#<0.55) at Little Sitkin and Great Sitkin (Fig. 2C). It is equally clear that despite experimental data indicating that calc-alkaline differentiation at Buldir requires saturation in spinel and hornblende near the liquidus (Waters et al., 2021), fractionation of amphibole alone cannot produce declining Mo abundances in Buldir samples which are clearly linked to decreasing Mg# from 0.65 to 0.45 (Fig. 2B). Thus, we conclude that fractional crystallization of amphibole is unlikely to be the main parameter controlling the observed Mo and B concentrations in Buldir. We infer instead that there are source variability and mixing effects at Buldir, which are evident in widely variable $^{87}Sr/^{86}Sr$ (Fig. 4E) and are common among the western Aleutian seafloor lavas (Yogodzinski et al., 2015, 2017), but are not reflected in Mo isotope data presented here.

In contrast to the western sample set, the near constant (and low) Mo/Ce, but high and variable B/Ce in the eastern samples require a combination of effects from differentiation in the presence of an anhydrous mineral assemblage and source variability in primitive samples (Mg#>0.60). Plots of B/Ce versus SiO_2 and MgO indicate that B/Ce nearly doubles during the evolution of Korovin samples from high-Al basalt to dacite (MgO from ~5.7 to 1.7 wt% – Fig. S5). Roughly constant Mo/Ce in the same sample set indicates the Mo and Ce are similarly incompatible in Korovin. The greater variability in B/Ce expressed in primitive basalts from Okmok (B/Ce ~1.2) and Seguam (B/Ce ~2.6) must reflect B enrichment in the source which peaks at Seguam, located just east of ~173° W where the AFZ enters the trench (Fig. 4). Based on the high $^{207}Pb/^{204}Pb$ and $^{87}Sr/^{86}Sr$ in arc lavas near the AFZ, Singer et al. (1996, 2007) argued for a direct link of greater sedimentary input to subduction of the AFZ. However, Singer et al. (2007) also speculated that the high B concentrations and high $^{87}Sr/^{86}Sr$ observed in volcanic rocks near the AFZ could reflect input not from sediment but from dehydration of subducted serpentinite or AOC. This point is discussed further below.

4.2. Source of high Mo and Mo/Ce in the western samples

Western Aleutian samples have $\delta^{98/95}Mo$ values that range from −0.38 to +0.01‰ (Fig. 2A) with an average ($\delta^{98/95}Mo = -0.16 \pm 0.09$‰) identical to that of MORB ($\delta^{98/95}Mo = -0.17$‰, Bezard et al., 2016; Chen et al., 2022; Hin et al., 2022). This is true even though primitive western Aleutian samples with Mg#>0.60 (Buldir Island, Ingenstrem Depression, Western Cones, Piip Seamount) have Mo concentrations (>1.0 μg/g) and Mo/Ce (>0.02) that are significantly greater than MORB (Figs. 2C and 5).

Molybdenum is widely interpreted as a fluid-mobile element in subduction systems (Bali et al., 2012) and enrichment in Mo has been linked to sources in subducted sediments (Casalini et al., 2019) and subducted oceanic crust (Freymuth et al., 2015). However, AOC and sediments cannot be key sources of Mo in the westernmost Aleutians (Piip, W. Cones, Ing. Depression and Buldir), because the $\delta^{98/95}Mo$ values of Aleutian sediments (down to −1.95‰) and AOC (−0.32 to −0.47‰,) are far lower than MORB and because the sample set also includes the Mg-andesites/dacites with the most unradiogenic MORB-like $^{87}Sr/^{86}Sr$ and $^{207}Pb/^{204}Pb$ in the arc (Yogodzinski et al., 2015, 2017). Conversely, based on the radiogenic $^{207}Pb/^{204}Pb$ values, sediments are clearly involved in Great Sitkin, Moffet and Kanaga (Fig. 4A). Given the extremely low $\delta^{98/95}Mo$ of Aleutian sediments, if Mo is mobilized from sediment sources, arc lavas from these volcanoes ought to have Mo isotopes lighter than MORB. However, Great Sitkin, Moffet and Kanaga have MORB-like Mo isotopes like those from the westernmost lavas (Fig. 4C), suggesting that Mo is not mobilized from sediments. We cannot exclude the possibility that Mo isotope fractionation occurs during sediment and/or AOC melting or dehydration, potentially leading to the MORB-like $\delta^{98/95}Mo$ of all western lavas. However, based on the lack of systematic change of $\delta^{98/95}Mo$ along the western part of the arc that contrasts the along-arc changes in Pb, Sr and Nd isotopes (tracing the sediment delivery into the trench, Fig. 4 – Kelemen et al., 2003; Yogodzinski et al., 2010), and the unradiogenic $^{87}Sr/^{86}Sr$ of western lavas, the dominant source of Mo enrichment in the western samples is unlikely to be subducted sediment or AOC.

The combined constraints from $\delta^{98/95}Mo$ and radiogenic isotopes indicate that the source of Mo in western Aleutian samples is most likely to be subducted Pacific MORB that has been little altered by seawater but that has been modified by some enrichment processes to produce the high Mo/Ce ratios. If correct, the process that produces Mo/Ce higher than MORB in the western Aleutians (Fig. 5) is likely to be the partial melting of subducted MORB under eclogite facies. This can be inferred from the Pb and Sr systematics of adakitic Mg-dacites of the Western Cones, which have the least radiogenic Pb and Sr isotopes in the arc ($^{87}Sr/^{86}Sr$ <0.7027, $^{207}Pb/^{204}Pb$ of ~15.455) but strongest Pb–Sr enrichments relative to the light rare-earth elements (LREE) (Ce/Pb <5, Nd/Sr <0.01– Yogodzinski et al., 2015, 2017). Fractionation of Ce/Pb and Nd/Sr is interpreted to reflect melting of the eclogitized oceanic crust (hereafter as MORB-type eclogite) at temperatures <900°C under water-saturated conditions and in the presence of garnet, rutile, and an additional LREE-rich accessory mineral (Klimm et al., 2008; Li et al., 2022; Yogodzinski et al., 2015). Water needed to drive melting of MORB-type eclogite is thought to be produced by dehydration of serpentinized peridotite in the mantle section of the subducting plate (e.g., Yogodzinski et al., 2017). This model for slab-melting works from an isotopic standpoint because fluids from serpentinite contribute small portions of the budgets for Sr, Pb, and by inference Mo. This is because only ~2% H_2O is needed to trigger up to 20% melting of subducted MORB (Schmidt et al., 2004). Elemental budgets in the resulting slab melt, especially at 5-10% melting, are dominated by the MORB-type eclogite which is isotopically (e.g., Sr, Nd, Pb isotopes) similar to depleted mantle (e.g., Li et al., 2022; Yogodzinski et al., 2015). Yogodzinski et al. (2017) outlined mass balance for Sr, and we infer here a similar mass balance for Mo.

A key aspect of our Mo concentration and isotope data and resulting model is that Mo is mobilized out of the subducting oceanic crust and incorporated into the source of Aleutian magmas somewhat more efficiently than Ce. This is surprising because rutile is present as a residual phase in the western Aleutians and a variety of observations argue that Mo is strongly compatible in rutile over Ce, hosting up to 30% of the Mo budget in a typical eclogite (Bali et al., 2012; Chen et al., 2019; Skora et al., 2017; Zack et al., 2002). Therefore, western Aleutian lavas, especially the adakitic Mg-andesites/dacites, ought to be depleted in Mo in a way that is comparable to Nb and Ta. However, trace element patterns of Aleutian lavas normalized to primitive mantle show enrichments in Mo relative to La and Ce (Fig. 5). This might suggest that rutile was not a residual phase following MORB-type eclogite melt extraction, but this is unlikely because adakitic Mg-andesites/dacites have large Ti,

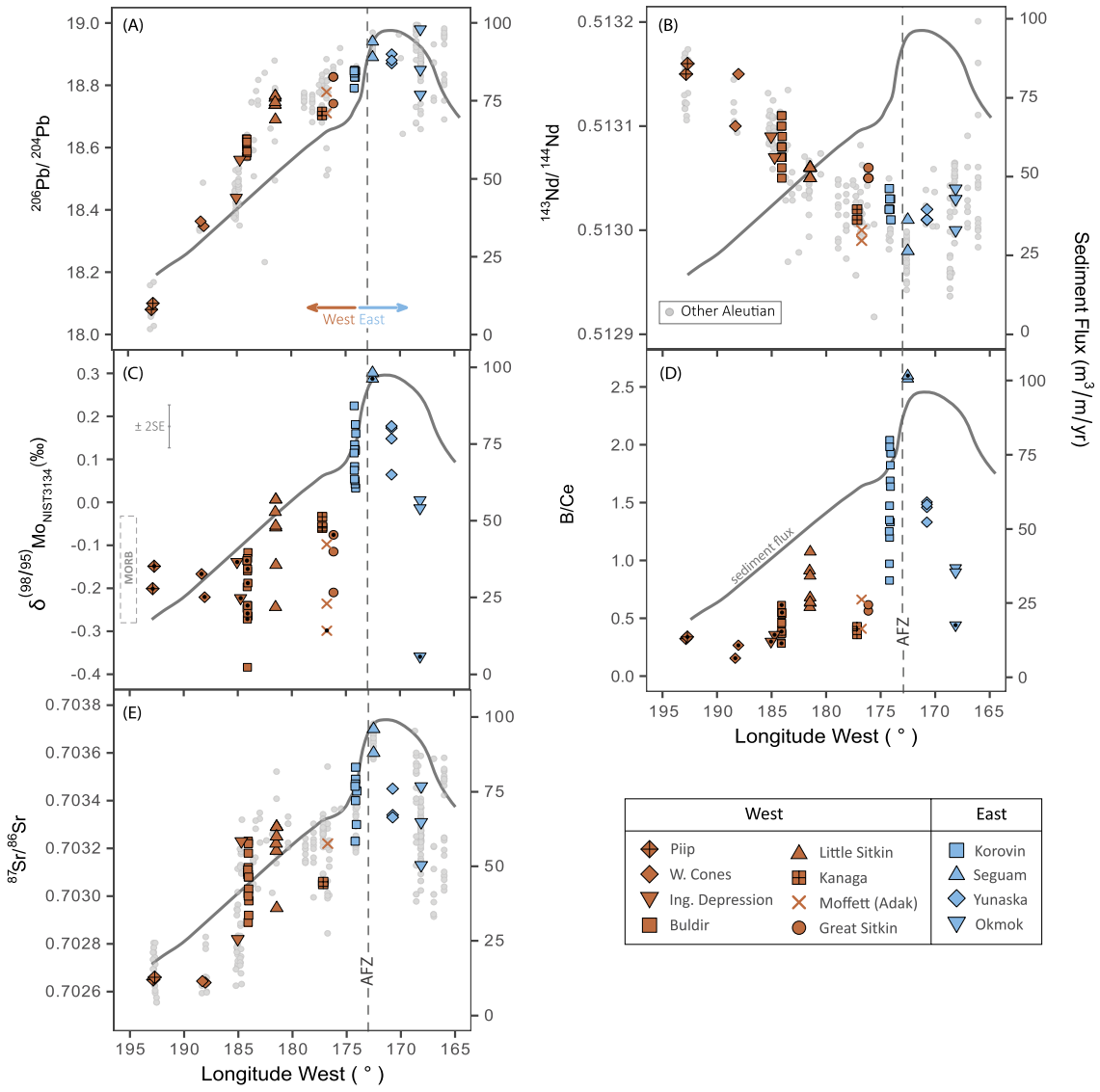

Fig. 4. Along-arc variance on Aleutian lavas isotope signatures. **(A)** Along arc $^{206}Pb/^{204}Pb$, **(B)** $^{143}Nd/^{144}Nd$, **(C)** $\delta^{98/95}Mo$ and **(D)** B/Ce ratios vs. Longitude West. Bold gray line represents sediment flux ($m^3/m/yr$) estimates from Kelemen et al. (2003). Dashed gray line shows the location of the Amlia Fracture Zone (AFZ) in the Aleutian arc. Sr-Nd-Pb isotope and Ce data for all Aleutian volcanoes from Singer et al. (2007); Arndt, 2011; Yogodzinski et al. (2010, 2015, 2017). Dashed gray rectangle in Fig. 4C represents the general $\delta^{98/95}Mo$ distribution for MORB (Bezard et al., 2016; Chen et al., 2022; Hin et al., 2022). Gray bar represents analytical uncertainty (±2SD) of ±0.05‰.

Ta, and Nb anomalies (e.g., elevated Eu/Ti and La/Nb) and high SiO_2 and Al_2O_3 contents collectively indicating rutile-saturated conditions at 800–900 °C (Hayden and Watson, 2007; Yogodzinski et al., 2015) consistent with hydrous melting of MORB under eclogite facies conditions (Carter et al., 2015; Klimm et al., 2008; Li et al., 2022).

Rutile present in the eclogitic slab is thought to retain a significant portion of Mo (Chen et al., 2019; Skora et al., 2017) and preferentially incorporate light Mo isotopes (Chen et al., 2019; Freymuth et al., 2015). Thus, if rutile controls the Mo budget in the source of the western Aleutian lavas, these should have low Mo concentrations and heavy Mo isotopes. However, we observe the opposite; elevated Mo/Ce ratios (Figs. 2C and 5) and low, MORB-like Mo isotopes (Fig. 4C). Available melting experiments indicate that the Mo partitioning in rutile is redox dependent. Chen et al. (2019) suggest significant Mo transport in fluids at oxygen fugacities above QFM +2 and Bali et al., (2012) show efficient mobilization of Mo in fluids from MORB-type eclogite with ~2 wt% rutile under oxidizing conditions (QFM +1.74). Similarly, melting experiments of AOC at 3 GPa and 750–900 °C suggest significant incorporation into rutile only at suitable reducing conditions (Skora et al., 2017). Oxidizing conditions like those in the Bali et al., (2012) experiments are consistent with conditions proposed for most Aleutian volcanoes (QFM +1.2 to +1.8; Zimmer et al., 2010; Waters et al., 2021) and are within the expected range of 1-5 log units above QFM of fluids during dehydration of serpentinite in subduction zones (Debret et al., 2016). Therefore, the expected compatible behavior of Mo in rutile might be counteracted if eclogite melting takes place under oxidizing conditions, like those expected for the Aleutian source.

It is nevertheless possible that residual rutile controls some of the Mo budget and, by inference, the Mo isotope composition of the erupted lavas. In that case, the measured Mo isotopes in the western Aleutian lavas may originate from a source that is much lighter than MORB (e.g., rutile in a dehydrated eclogitic slab) and only fortuitously happened to overlap the MORB range (Figs. 3 and 4C). While such a scenario is plausible, the lack of any systematic variation of Mo isotopes between the adakitic Mg-andesites/dacites (with a stronger slab component) and remaining western lavas (Fig. 4C) precludes us from placing any additional constraints to

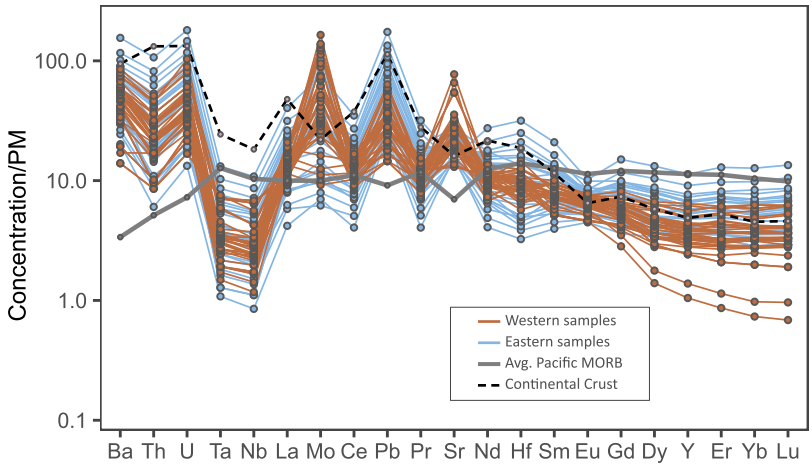

Fig. 5. Trace element concentrations relative to Primitive Mantle. Light blue lines represent eastern lavas (see main text for details on sample grouping), orange lines represent western lavas excepting Little Sitkin (where the REE plot patterns are instead explain by amphibole fractionation). Bold gray and black dashed lines show estimates for average MORB (Bezard et al., 2016; Chen et al., 2022; Hin et al., 2022) and continental crust (Rudnick and Gao, 2003). Aleutian data from Yogodzinski et al. (2010, 2015) and Arndt (2011). Primitive mantle values from McDonough and Sun (1995).

Table 1
Input compositions for $\delta^{98/95}$Mo vs. ^{206}Pb $/^{204}$Pb mixing calculations – sediment sources.

Endmember	$\delta^{98/95}$Mo (‰)	Mo (μg/g)	^{206}Pb $/^{204}$Pb	Pb (μg/g)
DM[a]	−0.20	0.025	18.20	0.023
Eclogite melt (SO201-1b-36-007)[b]	−0.22	3.45	18.34	4.1
Terrigenous sediment (183 38R 2 68-70)[c]	+0.17	1.21	19.04	12.9
Shale[d]	+0.55	51	21.69	6.3

[a] Mo data from McCoy-West et al., (2019), Pb isotope compositions from Yogodzinski et al., (2015) and Pb concentrations from Salters and Stracke (2004).
[b] Pb data from Yogodzinski et al., (2015).
[c] Pb data for DSDP 183 sediments from bulk sediment compositions in Plank and Langmuir (1998).
[d] Shale sediment composition from Freymuth et al., (2016).

such a model. Thus, we suggest that the MORB-like $\delta^{98/95}$Mo, coupled with enrichments in Mo over Ce (Mo/Ce>1.0) in the western Aleutian lavas imply extraction of Mo from the subducting plate under oxidizing conditions under which Mo is incompatible in the slab (Bali et al., 2012; Skora et al., 2017).

4.3. Source of Mo and B/Ce at the Amlia Fracture Zone

Korovin, Seguam, and Yunaska volcanoes have distinctly heavy Mo isotopes and high B/Ce ($\delta^{98/95}$Mo +0.03 to +0.30‰, B/Ce= 1.20–2.60), that decrease toward Okmok, which is the easternmost volcano of our study ($\delta^{98/95}$Mo = −0.12‰ and B/Ce ∼ 0.76, on average) (Figs. 4C-D). From this, it is clear that collectively, Mo, and B, are tracing the same source and that a particular and localized endmember with high $\delta^{98/95}$Mo and B/Ce is present at the AFZ. Singer et al. (1996) identified an enhanced role for subducted sediment in the source of volcanic rocks from Seguam Island. They initially attributed this to subduction of the AFZ and later expanded their interpretation to include enhanced fluid production by dehydration of subducted serpentinized peridotite (Singer et al., 1996, 2007). Based on this, it seems likely that the high $\delta^{98/95}$Mo and high B/Ce in the Korovin, Seguam, and Yunaska samples must be related to source characteristics of a particular subducted sediment at the AFZ or serpentinized peridotite, or both.

We explore the possible source mixtures that invoke subducted sediment to explain the isotopically heavy Mo in samples from Korovin, Seguam and Yunaska, near the AFZ (hereafter also as AFZ lavas) with mixing calculations in a $\delta^{98/95}$Mo-^{206}Pb/^{204}Pb space (as Pb isotopes trace the sediment sources in Aleutian rocks)

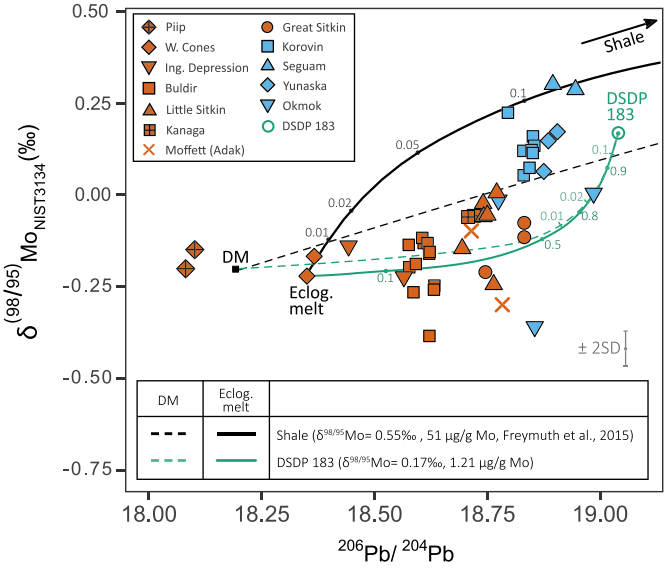

Fig. 6. Mixing calculations between DM (Depleted Mantle), eclogite melts (SO201-1b-36-007), DSDP 183 and shale-like sediments, Aleutian arc. $\delta^{98/95}$Mo vs. ^{207}Pb/^{204}Pb. Green line shows mixing with the sole high $\delta^{98/95}$Mo DSDP 183 sediment sample (Plank and Langmuir, 1998; this study). Black lines show mixing with black shales (Freymuth et al., 2015). Solid and dashed lines represent mixing of eclogite melts (using the SO201-1b-36-007 Western Cones sample, Yogodzinski et al., 2015; this study) and upper mantle (DM). Mantle Mo data from McCoy-West et al., (2019), Pb isotope compositions from Yogodzinski et al., (2015) and Pb concentrations from Salters and Stracke (2004). See Table 1 for details on input compositions. Gray bar represents analytical uncertainty (±2SD) of ±0.05‰.

(Fig. 6). For the MORB-like components we use eclogite melts using the SO201-1b-36-007 Western Cones sample, and depleted mantle (DM) (input compositions in Table 1). Mixing lines from these endmembers to the DSDP 183 sample with highest $\delta^{98/95}$Mo (+0.17‰) have the expected concave-up curvature of the Aleutian lavas, but the $\delta^{98/95}$Mo in the sediment is too low to explain the full range of the AFZ lavas compositions. Organic-rich shales (black shales) carry higher $\delta^{98/95}$Mo (up to +0.55‰), but also significantly higher Mo concentrations (51 μg/g) (Freymuth et al., 2016). Mixing with black shales produces lines that pass through the AFZ lavas, but their high Mo concentrations produce straight or concave-down mixing lines that are inconsistent with the broad upward curvature of the AFZ lavas pattern. More impor-

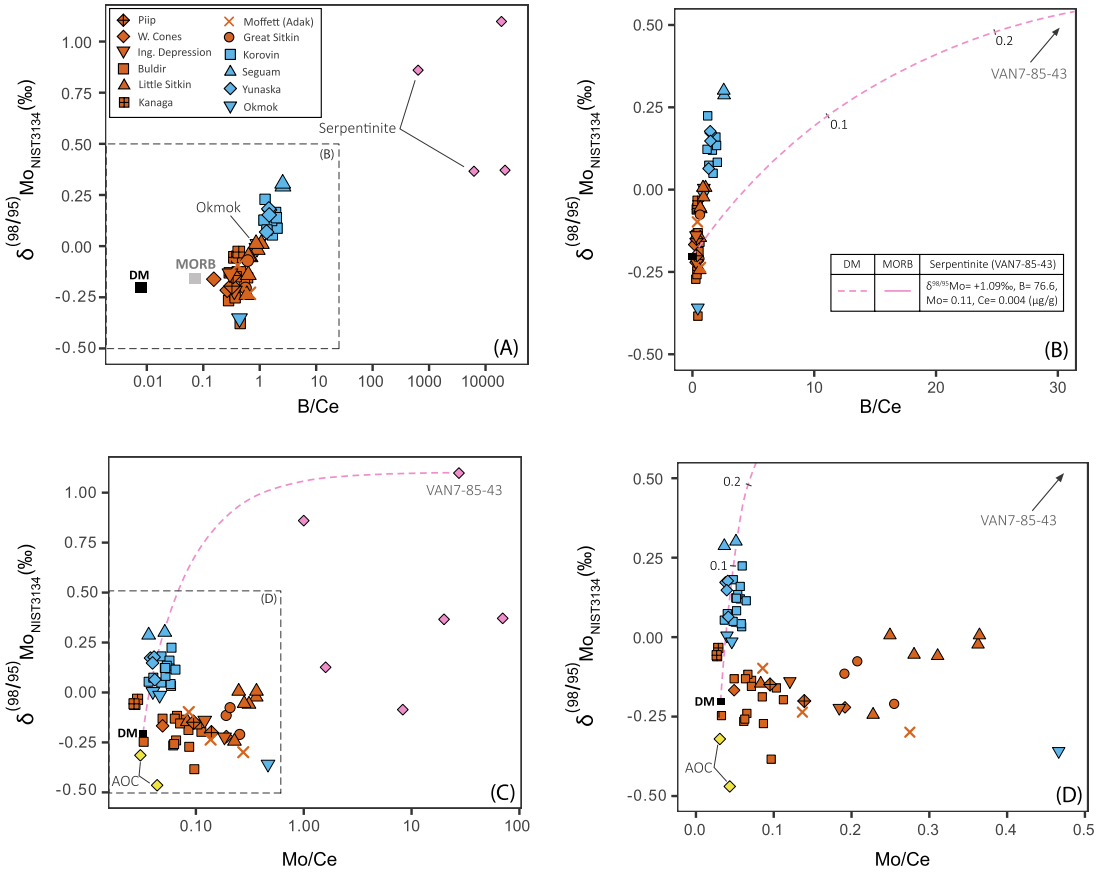

Fig. 7. Mo isotopes vs. B/Ce and Mo/Ce ratios for Aleutian lavas, serpentinized peridotites and AOC. **(A)** $\delta^{98/95}$Mo vs. B/Ce for Aleutian lavas (see legend in the left upper corner), average MORB (gray square, Bezard et al., 2016; Chen et al., 2022; Hin et al., 2022), DM (Salters and Stracke, 2004; McCoy-West et al., 2019), serpentinized peridotites (magenta diamonds, Frisby et al., 2016a; this study). Dashed rectangle shows the bounds of Fig. 7B. **(B)** Inset in Fig. 7A. **(C)** $\delta^{98/95}$Mo vs. Mo/Ce ratios for Aleutian lavas, serpentinized peridotites (magenta diamonds) and AOC (yellow diamonds). Dashed rectangle represents the bounds of Fig. 7D. **(D)** Inset in Fig. 7C. Magenta dashed lines in (B), (C) and (D) represent mixing calculations between bulk serpentinized peridotite (VAN-85-43) and DM. Numbers next to the lines show proportion of bulk serpentinite in the mix. See Table 2 and discussion for input compositions and references. Horizontal axes of Figs. 7A-C in logarithmic scale. Gray bar represents analytical uncertainty (±2SD) of ±0.05‰.

Table 2
Input compositions for $\delta^{98/95}$Mo vs. Mo/Ce and B/Mo mixing calculations – serpentinized peridotites.

Endmember	$\delta^{98/95}$Mo (‰)	Mo (µg/g)	Ce (µg/g)	B (µg/g)	B/Ce	Mo/Ce	B/Mo
DM[a]	−0.20	0.025	0.772	0.06	0.078	0.032	2.40
MORB[b]	−0.16	0.613	14.860	1.07	0.072	0.041	1.74
Serp. peridotite (VAN7-85-43)[c]	+1.09	0.11	0.004	76.6	19150	27.5	696

[a] Mo data from McCoy-West et al., (2019), Ce and B concentrations from Salters and Stracke (2004).
[b] Mo isotope data for MORB from Bezard et al., (2016), B from Marschall et al., (2017) and Ce from Gale et al., (2013).
[c] Ce and B concentrations from Frisby et al., (2016a).

tantly, organic-rich sediments are not present in significant quantities in the DSDP 183 core (Creager et al., 1973). It is possible that additional measurements of DSDP 183 samples will identify sediments with appropriately heavy Mo isotopes ($\delta^{98/95}$Mo > +0.30). However, the weighted average composition of the drill core must include significant quantities of Mo from pelagic sediment (Plank and Langmuir, 1998), which (based on our Site 886C results) carries far greater amounts of Mo that is isotopically far lighter (Fig. 3A). Thus, we conclude that average subducting Aleutian sediment is likely to carry Mo that is isotopically light ($\delta^{98/95}$Mo < −0.5), and that a distinctive sediment composition around the AFZ is unlikely to explain the isotopically heavy Mo in the AFZ lavas.

Serpentinized abyssal peridotites analyzed here have higher Mo concentrations (0.11–0.68 µg/g) than primitive mantle coupled to high $\delta^{98/95}$Mo (up to +1.09‰) approaching seawater (+2.09‰, Greber et al., 2012), and elevated B (70–89 µg/g), B/Ce (up to ~22000) and Mo/Ce (~3.8) (Figs. 3A-7) values. High B/Ce and Mo/Ce in serpentinized peridotites compared to primitive mantle (Fig. S6, 0.0002 and 0.03 respectively; McDonough and Sun, 1995) are analogous to the seawater-derived U and Sr enrichments (Frisby et al., 2016a). Moreover, the high $\delta^{98/95}$Mo in these samples are comparable to their seawater-like bulk rock Nd, Sr isotopes (Frisby et al., 2016b), suggesting that Mo and B are scavenged from seawater and that serpentinization leads to the observed heavy Mo isotopes. As such, serpentinites are likely to be more suitable sources for Mo and B in the AFZ lavas. Although it is quite clear that sediments are present in the source of the AFZ lavas (as evident with Pb-Nd isotopes and the high sediment flux near the AFZ), the particularly high $\delta^{98/95}$Mo and B/Ce in arc lavas near the AFZ suggest that serpentinite sources must overwhelm-

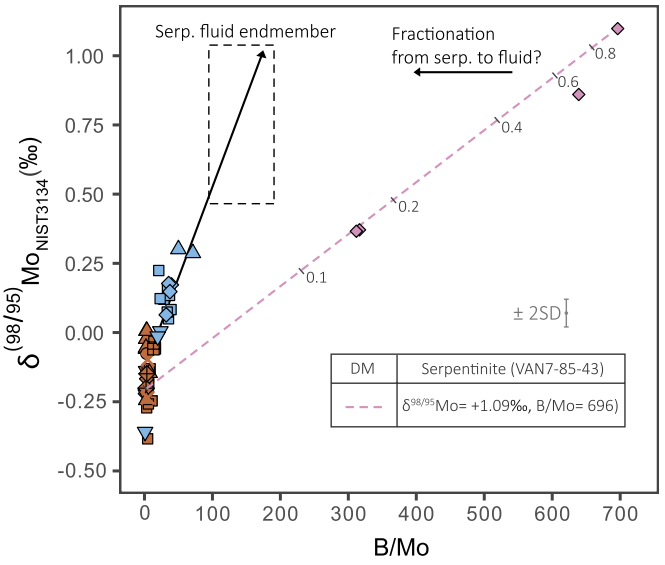

Fig. 8. Mo isotopes vs. B/Mo for Aleutian lavas and serpentinized peridotites. Magenta dashed line represents mixing calculations between DM (dashed) and bulk serpentinized peridotite (VAN7-85-43). Numbers represent the proportion of the serpentinized peridotite endmember in the mix. Dashed rectangle shows composition of the proposed serpentinite-derived fluid. Details of input endmembers outlined in Table 2. DM and serpentinized peridotite references as in Fig. 7. Gray bar represents analytical uncertainty (±2SD) of ±0.05‰.

ingly control the Mo isotope and B systematics in this area. The advantages of serpentinites as a localized source at the AFZ are clearly illustrated in mixing patterns between DM and bulk serpentinite (using VAN7-85-43 with $\delta^{98/95}$Mo= +1.09‰) in Figs. 7 and 8 (input compositions in Table 2). Figs. 7C-D show that mixing lines connecting bulk serpentinite to DM have concave downward curvatures that produce rapid growth in $\delta^{98/95}$Mo from the DM endmember at nearly constant Mo/Ce. Therefore, addition of ~10% of Mo from bulk serpentinized peridotite to a DM source matches closely the pattern expressed in AFZ lavas. However, the serpentinized peridotite-DM mixing results are less clear in $\delta^{98/95}$Mo vs. B/Ce space, as the serpentinized peridotites have B/Ce that are too high to explain the data (Fig. 7B). Mo, B, and Ce contents of serpentinites vary widely (Deschamps et al., 2013), but even so, the identical calculations using Mid Atlantic ridge and Hess Deep peridotites (Kodolányi et al., 2012), with 20-times lower B/Ce compared to SWIR peridotites, have B/Ce that are still too high to explain the data patterns (Fig. S7). An important implication from the mixing calculations is that a bulk serpentinized peridotite endmember explains the Mo, but not the B systematics of the AFZ lavas. This suggests some decoupling (in terms of partitioning) between B and Mo during mobilization from the serpentinized peridotites into the source of AFZ lavas.

The high $\delta^{98/95}$Mo at the AFZ lavas (approaching the SWIR serpentinized peridotites) indicate that Mo must be predominantly sourced in serpentinite. However, the observed decoupling between Mo and B imply that the "serpentinite component" may not be represented by bulk rock. Dehydration of serpentinite is thought to be a key mechanism of fluid flux in arc systems (e.g., Schmidt and Poli, 2003). Therefore, fluids derived by serpentinite dehydration may represent a more appropriate high $\delta^{98/95}$Mo-B/Ce endmember for the AFZ lavas. To explore the Mo and B behavior in this fluid, without the Ce concentration compounding uncertainties, we provide similar mixing calculations (between DM and VAN7-85-43, Table 2) using B/Mo. Eastern samples have high B/Mo and display a linear correlation with $\delta^{98/95}$Mo, implying that a single, high B/Mo, component is involved (Fig. 8). Mixing between DM and bulk serpentinized peridotite also produces linear mixing trends, yet the B/Mo of the latter is too high to explain the AFZ lavas. Assuming that the Mo isotope composition of the serpentinite-derived fluid is identical to that of the bulk serpentinized peridotite, by extrapolating from the bulk peridotites, a more fitting serpentinite component must have 2–3 times lower B/Mo (~150–200) than bulk serpentinized peridotites analyzed here (~650–700) (Fig. 8). This suggests that, upon dehydration, Mo is 2–3 times more efficiently partitioned into the fluid relative to B. Using a $D_B^{fluid/solid} = 4$ during serpentinite dehydration (Tenthorey and Hermann, 2004), the partition coefficient for Mo should be $D_{Mo}^{fluid/solid}$= 8–12. If true, this inferred higher Mo flux during serpentinite dehydration would be qualitatively consistent with significant retention of B in chlorite past the antigorite stability field and beyond the arc magma sources in dehydrated peridotites (Scambelluri et al., 2004). However, experimental data are critically needed to understand the Mo behavior during serpentinite dehydration.

Finally, the combined Mo isotope and B concentration data indicate that there is an enhanced role for serpentinite-derived fluids in the source of the AFZ volcanoes. However, it is not entirely clear how or why subduction of the AFZ produces this effect. Faulting, fluid-ingress and serpentinization in the mantle section of the subducting plate (Ranero et al., 2003) should be common throughout the Aleutian island-arc (Shillington et al., 2015). We have already invoked dehydration of serpentinite produced in this way as the source of fluid that drives melting of the subducting oceanic crust to create high Mo/Ce in the western samples which have $\delta^{98/95}$Mo little different from that of MORB (Section 4.2 above). We assume this process must be happening throughout the Aleutian system. If so, what mechanism produces an enhanced role for serpentinite-derived Mo and heavy Mo isotopes in the AFZ volcanoes?

One possibility is that the AFZ allows greater seawater infiltration and thus extensive serpentinization of the subducting upper mantle. Then, in contrast to the western portion of the arc, subsequent dehydration of the subducting mantle may lead to greater fluid production and more direct incorporation of serpentinite-derived fluids into the arc sources, both at and due the AFZ. Alternatively, serpentinization of the subducting lithosphere may create fluid pathways that trigger hydration and serpentinite formation in the subduction channel above the down-going plate. Indeed, serpentinite above the plate interface, which is produced initially beneath the forearc and is dragged to depth above the subducting oceanic crust (e.g., Bostock et al., 2002; Savov et al., 2007) is a different potential source of serpentinite-derived fluids that has not been previously discussed here and which does not seem to play a significant role in the control of Mo systematics outside of the AFZ area. Subduction-channel serpentinite may be enhanced at the AFZ, or alternatively the offset on the subducting seafloor might create a physical trap that captures a greater thickness of subduction-channel serpentinite as the AFZ passes beneath the forearc. Whatever the physical-chemical mechanism, the combined Mo isotope and B concentration datasets provide a unique insight confirming previous work (Singer et al., 1996, 2007) indicating that serpentinite-derived fluids play an enhanced role in the composition of the Aleutian source below the AFZ volcanoes.

5. Conclusions

The distinct $\delta^{98/95}$Mo values in Korovin and Buldir indicate that calc-alkaline magmatic differentiation, with or without amphibole, does not produce Mo isotopic fractionation. Instead, the Mo isotope systematics are tracing source characteristics. Contrasting patterns between along-arc $\delta^{98/95}$Mo, ^{143}Nd/^{144}Nd, ^{206}Pb/^{204}Pb, and sediment flux, and low $\delta^{98/95}$Mo in Pacific sediments and AOC analyzed here indicate that the Mo fluxes are not controlled by subducted sediment or AOC in the Aleutian arc. Rather, low MORB-like

$\delta^{98/95}$Mo, but high Mo/Ce in the western Aleutian lavas suggest that Pacific MORB sources control the Mo budget with nearly absent Mo isotope fractionation from the slab to the arc lavas. Highly oxidizing conditions are likely responsible for the diminished role of rutile in retaining Mo and hence high Mo/Ce ratios in the western samples. In turn, the high $\delta^{98/95}$Mo, B/Mo and B/Ce ratios of Korovin, Seguam and Yunaska are best explained by serpentinite-derived fluid addition. Production of serpentinite fluids is likely via dehydration of Pacific lithosphere that either leads to a direct fluid incorporation into the arc sources or formation of forearc serpentinite in the subduction channel (both due to the AFZ). From mixing calculations, it appears that this fluid ought to have 2–3 times higher Mo than B, suggesting preferential partitioning of Mo (than B) into a serpentinite-derived fluid. The resulting data highlights that the combined Mo–B systematics can be used as a useful proxy for tracing fluid sources in subduction zones and provides evidence for serpentinites as an additional heavy Mo isotopes-component in subduction zones that might not have been previously considered.

CRediT authorship contribution statement

Ekaterina Rojas-Kolomiets: Conceptualization, Data curation, Formal analysis, Investigation, Methodology, Validation, Visualization, Writing – original draft. **Owen Jensen:** Data curation, Formal analysis, Investigation, Writing – original draft, Writing – review & editing. **Michael Bizimis:** Conceptualization, Funding acquisition, Methodology, Resources, Supervision, Validation, Writing – review & editing. **Gene Yogodzinski:** Conceptualization, Funding acquisition, Supervision, Writing – review & editing. **Lukáš Ackerman:** Methodology, Resources, Validation, Writing – review & editing.

Declaration of competing interest

The authors declare that they have no known competing financial interests or personal relationships that could have influenced the work reported in this study.

Data availability

Data is available as an Excel file in the supplementary materials.

Acknowledgements

We acknowledge that the Aleutian Islands (Unangam Tanangin) are the original homeland of the Unangax̂ and Alutiiq/Sugpiaq people on which our work occurs and to whom we owe gratitude. We acknowledge the painful history of colonization and genocide in this are area and the resilience of the Alutiiq and Unangax̂ families. We also recognize that the names of the Aleutian Islands reported in this study are not necessarily the original names given by the Unangax̂ and Alutiiq/Sugpiaq people. This study was funded by US National Science Foundation grants EAR 2050271 awarded to M. Bizimis and G. Yogodzinski and OCE 1551640 and EAR 1753518 awarded to G. Yogodzinski. We thank Jim Sexton, CEMS lab manager, for assistance with data analyses. LA acknowledges the institutional support RVO67985831 of the Institute of Geology of the Czech Academy of Sciences. We thank the Associate Editor Dr. Hickey-Vargas for efficient handling of the paper. Helpful reviews by two anonymous reviewers are also gratefully acknowledged.

Appendix A. Supplementary material

Supplementary material related to this article can be found online at https://doi.org/10.1016/j.epsl.2022.117970.

References

Ahmad, Q., Wille, M., König, S., Rosca, C., Hensel, A., Pettke, T., Hermann, J., 2021. The Molybdenum isotope subduction recycling conundrum: A case study from the Tongan subduction zone, Western Alps and Alpine Corsica. Chem. Geol. 576, 120231. https://doi.org/10.1016/j.chemgeo.2021.120231.

Arndt, S., 2011. Controls of Melt Genesis and Evolution at Buldir Volcano in the Western Aleutian Island Arc. Master's thesis. University of South Carolina.

Bali, E., Keppler, H., Audetat, A., 2012. The mobility of W and Mo in subduction zone fluids and the Mo–W–Th–U systematics of island arc magmas. Earth Planet. Sci. Lett. 351–352, 195–207. https://doi.org/10.1016/j.epsl.2012.07.032.

Bezard, R., Fischer-Gödde, M., Hamelin, C., Brennecka, G.A., Kleine, T., 2016. The effects of magmatic processes and crustal recycling on the molybdenum stable isotopic composition of Mid-Ocean Ridge Basalts. Earth Planet. Sci. Lett. 453, 171–181. https://doi.org/10.1016/j.epsl.2016.07.056.

Bostock, M.G., Hyndman, R.D., Rondenay, S., Peacock, S.M., 2002. An inverted continental Moho and serpentinization of the forearc mantle. Nature 417 (6888), 536–538. https://doi.org/10.1038/417536a.

Burkhardt, C., Hin, R.C., Kleine, T., Bourdon, B., 2014. Evidence for Mo isotope fractionation in the solar nebula and during planetary differentiation. Earth Planet. Sci. Lett. 391, 201–211. https://doi.org/10.1016/j.epsl.2014.01.037.

Carter, L.B., Skora, S., Blundy, J.D., De Hoog, J.C.M., Elliott, T., 2015. An experimental study of trace element fluxes from subducted oceanic crust. J. Petrol. 56 (8), 1585–1606. https://doi.org/10.1093/petrology/egv046.

Casalini, M., Avanzinelli, R., Tommasini, S., Elliott, T., Conticelli, S., 2019. Ce/Mo and molybdenum isotope systematics in subduction-related orogenic potassic magmas of Central-Southern Italy. Geochem. Geophys. Geosyst. 20 (6), 2753–2768. https://doi.org/10.1029/2019GC008193.

Chen, S., Hin, R.C., John, T., Brooker, R., Bryan, B., Niu, Y., Elliott, T., 2019. Molybdenum systematics of subducted crust record reactive fluid flow from underlying slab serpentine dehydration. Nat. Commun. 10 (1), 4773. https://doi.org/10.1038/s41467-019-12696-3.

Chen, S., Sun, P., Niu, Y., Guo, P., Elliott, T., Hin, R.C., 2022. Molybdenum isotope systematics of lavas from the East Pacific rise: constraints on the source of enriched mid-ocean ridge basalt. Earth Planet. Sci. Lett. 578, 117283. https://doi.org/10.1016/j.epsl.2021.117283.

Creager, J.S., Scholl, D.W., Boyce, R.E., Echols, R.J., Lee, H.J., Ling, H.Y., Stewart, R.J., Supko, P.R., Worsley, T.R., 1973. Deep sea drilling project. Site Report, Site 183. https://doi.org/10.2973/dsdp.proc.19.102.1973.

Debret, B., Millet, M.-A., Pons, M.-L., Bouilhol, P., Inglis, E., Williams, H., 2016. Isotopic evidence for iron mobility during subduction. Geology 44 (3), 215–218. https://doi.org/10.1130/G37565.1.

Deschamps, F., Godard, M., Guillot, S., Hattori, K., 2013. Geochemistry of subduction zone serpentinites: a review. Lithos 178, 96–127. https://doi.org/10.1016/j.lithos.2013.05.019.

Freymuth, H., Elliott, T., van Soest, M., Skora, S., 2016. Tracing subducted black shales in the Lesser Antilles arc using molybdenum isotope ratios. Geology 44 (12), 987–990. https://doi.org/10.1130/G38344.1.

Freymuth, H., Vils, F., Willbold, M., Taylor, R.N., Elliott, T., 2015. Molybdenum mobility and isotopic fractionation during subduction at the Mariana arc. Earth Planet. Sci. Lett. 432, 176–186. https://doi.org/10.1016/j.epsl.2015.10.006.

Frisby, C., Bizimis, M., Mallick, S., 2016a. Seawater-derived rare Earth element addition to abyssal peridotites during serpentinization. Lithos 248–251, 432–454. https://doi.org/10.1016/j.lithos.2016.01.025.

Frisby, C., Bizimis, M., Mallick, S., 2016b. Hf–Nd isotope decoupling in bulk abyssal peridotites due to serpentinization. Chem. Geol. 440, 60–72. https://doi.org/10.1016/j.chemgeo.2016.07.006.

Gale, A., Dalton, C.A., Langmuir, C.H., Su, Y., Schilling, J.-G., 2013. The mean composition of ocean ridge basalts. Geochem. Geophys. Geosyst. 14 (3), 489–518. https://doi.org/10.1029/2012GC004334.

Gaschnig, R.M., Reinhard, C.T., Planavsky, N.J., Wang, X., Asael, D., Chauvel, C., 2017. The Molybdenum isotope system as a tracer of slab input in subduction zones: an example from Martinique, Lesser Antilles arc. Geochem. Geophys. Geosyst. 18 (12), 4674–4689. https://doi.org/10.1002/2017GC007085.

Gaspers, N., Magna, T., Ackerman, L., 2020. Molybdenum mass fractions and stable isotope compositions of sedimentary carbonate and silicate reference materials. Geostand. Geoanal. Res. 44 (2), 363–374. https://doi.org/10.1111/ggr.12314.

Gill, J.B., 1981. Orogenic Andesites and Plate Tectonics, 1st ed. Springer Verlag, Berlin.

Greber, N.D., Siebert, C., Nägler, T.F., Pettke, T., 2012. δ98/95Mo values and Molybdenum concentration data for NIST SRM 610, 612 and 3134: towards a common protocol for reporting Mo data. Geostand. Geoanal. Res. 36 (3), 291–300. https://doi.org/10.1111/j.1751-908X.2012.00160.x.

Hayden, L.A., Watson, E.B., 2007. Rutile saturation in hydrous siliceous melts and its bearing on Ti-thermometry of quartz and zircon. Earth Planet. Sci. Lett. 258 (3–4), 561–568. https://doi.org/10.1016/j.epsl.2007.04.020.

Hin, R.C., Hibbert, K.E.J., Chen, S., Willbold, M., Andersen, M.B., Kiseeva, E.S., Wood, B.J., Niu, Y., Sims, K.W.W., Elliott, T., 2022. The influence of crustal recycling on the molybdenum isotope composition of the Earth's mantle. Earth Planet. Sci. Lett. 595, 117760. https://doi.org/10.1016/j.epsl.2022.117760.

Jicha, B.R., Singer, B.S., Brophy, J.G., Fournelle, J.H., Johnson, C.M., Beard, B.L., Lapen, T.J., Mahlen, N.J., 2004. Variable impact of the subducted slab on Aleutian Island Arc magma sources: evidence from Sr, Nd, Pb and Hf isotopes and trace element abundances. J. Petrol. 45, 1845–1875.

Kay, S.M., Kay, R.W., 1985. Aleutian tholeiitie and cale-alkaline magma series I: the mafic phenocrysts. Contrib. Mineral. Petrol. 90, 276–290.

Kelemen, P.B., Yogodzinski, G.M., Scholl, D.W., 2003. Along-strike variation in the Aleutian Island Arc: Genesis of high Mg# andesite and implications for continental crust. In: Eiler, J. (Ed.), Geophysical Monograph Series, vol. 138. American Geophysical Union, pp. 223–276.

Klimm, K., Blundy, J.D., Green, T.H., 2008. Trace element partitioning and accessory phase saturation during H2O-saturated melting of basalt with implications for subduction zone chemical fluxes. J. Petrol. 49, 523–553. https://doi.org/10.1093/petrology/egn001.

Kodolányi, J., Pettke, T., Spandler, C., Kamber, B.S., Gméling, K., 2012. Geochemistry of ocean floor and fore-arc serpentinites: constraints on the ultramafic input to subduction zones. J. Petrol. 53 (2), 235–270. https://doi.org/10.1093/petrology/egr058.

König, S., Wille, M., Voegelin, A., Schoenberg, R., 2016. Molybdenum isotope systematics in subduction zones. Earth Planet. Sci. Lett. 447, 95–102. https://doi.org/10.1016/j.epsl.2016.04.033.

Li, H., Hermann, J., Zhang, L., 2022. Melting of subducted slab dictates trace element recycling in global arcs. Sci. Adv. 8 (2), eabh2166. https://doi.org/10.1126/sciadv.abh2166.

Liang, Y.-H., Halliday, A.N., Siebert, C., Fitton, J.G., Burton, K.W., Wang, K.-L., Harvey, J., 2017. Molybdenum isotope fractionation in the mantle. Geochim. Cosmochim. Acta 199, 91–111. https://doi.org/10.1016/j.gca.2016.11.023.

Marschall, H.R., Wanless, V.D., Shimizu, N., Pogge von Strandmann, P.A.E, Elliott, T., Monteleone, B.D., 2017. The boron and lithium isotopic composition of mid-ocean ridge basalts and the mantle. Geochim. Cosmochim. Acta 207, 102–138. https://doi.org/10.1016/j.gca.2017.03.028.

McCoy-West, A.J., Chowdhury, P., Burton, K.W., Sossi, P., Nowell, G.M., Fitton, J.G., Kerr, A.C., Cawood, P.A., Williams, H.M., 2019. Extensive crustal extraction in Earth's early history inferred from molybdenum isotopes. Nat. Geosci. 12 (11), 946–951. https://doi.org/10.1038/s41561-019-0451-2.

McDonough, W.F., Sun, S.S., 1995. The composition of the Earth. Chem. Geol. 120 (3–4), 223–253. https://doi.org/10.1016/0009-2541(94)00140-4.

Menard, G., Vlastélic, I., Ionov, D.A., Rose-Koga, E.F., Piro, J.L., Pin, C., 2013. Precise and accurate determination of boron concentration in silicate rocks by direct isotope dilution ICP-MS: insights into the B budget of the mantle and B behavior in magmatic systems. Chem. Geol. 354, 139–149. https://doi.org/10.1016/j.chemgeo.2013.06.017.

Nandedkar, R.H., Hürlimann, N., Ulmer, P., Müntener, O., 2016. Amphibole–melt trace element partitioning of fractionating calc-alkaline magmas in the lower crust: an experimental study. Contrib. Mineral. Petrol. 171 (8–9), 71. https://doi.org/10.1007/s00410-016-1278-0.

Plank, T., Langmuir, C.H., 1998. The chemical composition of subducting sediment and its consequences for the crust and mantle. Chem. Geol. 145 (3–4), 325–394. https://doi.org/10.1016/S0009-2541(97)00150-2.

Ranero, C.R., Phipps Morgan, J., McIntosh, K., Reichert, C., 2003. Bending-related faulting and mantle serpentinization at the Middle America trench. Nature 425 (6956), 367–373. https://doi.org/10.1038/nature01961.

Rea, D.K., Basov, I.A., Scholl, D.W., Allan, J.F. (Eds.) 1993. Proceedings of the Ocean Drilling Program, Scientific Results, vol. 145.

Rudge, J.F., Reynolds, B.C., Bourdon, B., 2009. The double spike toolbox. Chem. Geol. 265 (3–4), 420–431. https://doi.org/10.1016/j.chemgeo.2009.05.010.

Rudnick, R.L., 1995. Making continental crust. Nature 378, 571–578.

Rudnick, R.L., Gao, S., 2003. Composition of the continental crust. In: Rudnick, R.L. (Ed.), The Crust. Elsevier-Pergamon, Oxford, pp. 1–64.

Ryan, J.G., Chauvel, C., 2014. The subduction-zone filter and the impact of recycled materials on the evolution of the mantle. In: Holland, H.D., Turekian, K.K. (Eds.), 2nd edition. Treatise on Geochemistry, Vol. 3: The Mantle and Core. Elsevier, New York, pp. 479–508.

Salters, V.J.M., Stracke, A., 2004. Composition of the depleted mantle. Geochem. Geophys. Geosyst. 5 (5), 1–27. https://doi.org/10.1029/2003GC000597.

Savov, I.P., Ryan, J.G., D'Antonio, M., Fryer, P., 2007. Shallow slab fluid release across and along the Mariana arc-basin system: insights from geochemistry of serpentinized peridotites from the Mariana fore arc. J. Geophys. Res. 112 (B9), B09205. https://doi.org/10.1029/2006JB004749.

Scambelluri, M., Müntener, O., Ottolini, L., Pettke, T.T., Vannucci, R., 2004. The fate of B, Cl and Li in the subducted oceanic mantle and in the antigorite breakdown fluids. Earth Planet. Sci. Lett. 222 (1), 217–234. https://doi.org/10.1016/j.epsl.2004.02.012.

Schmidt, M.W., Poli, S., 2003. Generation of mobile components during subduction of oceanic crust. In: Treatise on Geochemistry, pp. 567–591.

Schmidt, M.W., Vielzeuf, D., Auzanneau, E., 2004. Melting and dissolution of subducting crust at high pressures: the key role of white mica. Earth Planet. Sci. Lett. 228 (1–2), 65–84. https://doi.org/10.1016/j.epsl.2004.09.020.

Scholl, D.W., Vallier, T.L., Stevenson, A.J., 1982. Sedimentation and deformation in the Amlia Fracture Zone sector of the Aleutian Trench. Mar. Geol. 48 (1–2), 105–134. https://doi.org/10.1016/0025-3227(82)90132-3.

Shillington, D.J., Bécel, A., Nedimović, M.R., Kuehn, H., Webb, S.C., Abers, G.A., Keranen, K.M., Li, J., Delescluse, M., Mattei-Salicrup, G.A., 2015. Link between plate fabric, hydration and subduction zone seismicity in Alaska. Nat. Geosci. 8 (12), 961–964. https://doi.org/10.1038/ngeo2586.

Siebert, C., Nägler, T.F., Kramers, J.D., 2001. Determination of molybdenum isotope fractionation by double-spike multicollector inductively coupled plasma mass spectrometry. Geochem. Geophys. Geosyst. 2. https://doi.org/10.1029/2000GC000124.

Singer, B.S., Jicha, B.R., Leeman, W.P., Rogers, N.W., Thirlwall, M.F., Ryan, J., Nicolaysen, K.E., 2007. Along-strike trace element and isotopic variation in Aleutian island arc basalt: subduction melts sediments and dehydrates serpentine. J. Geophys. Res. 112 (B6), B06206-26. https://doi.org/10.1029/2006JB004897.

Singer, B.S., Leeman, W.P., Thirlwall, M.F., Rogers, N.W., 1996. Does fracture zone subduction increase sediment flux and mantle melting in subduction zones? Trace element evidence from Aleutian Arc Basalt. In: Bebout, G.E., Scholl, D.W., Kirby, S.H., Platt, J.P. (Eds.), Geophysical Monograph Series. American Geophysical Union, pp. 285–291.

Skora, S., Freymuth, H., Blundy, J., Elliott, T., Guillong, M., 2017. An experimental study of the behaviour of cerium/molybdenum ratios during subduction: implications for tracing the slab component in the Lesser Antilles and Mariana Arc. Geochim. Cosmochim. Acta 212, 133–155. https://doi.org/10.1016/j.gca.2017.05.025.

Spandler, C., Pirard, C., 2013. Element recycling from subducting slabs to arc crust: a review. Lithos 170–171, 208–223. https://doi.org/10.1016/j.lithos.2013.02.016.

Tenthorey, E., Hermann, J., 2004. Composition of fluids during serpentinite breakdown in subduction zones: evidence for limited boron mobility. Geology 32 (10), 865. https://doi.org/10.1130/G20610.1.

Villalobos-Orchard, J., Freymuth, H., O'Driscoll, B., Elliott, T., Williams, H., Casalini, M., Willbold, M., 2020. Molybdenum isotope ratios in izu arc basalts: the control of subduction zone fluids on compositional variations in arc volcanic systems. Geochim. Cosmochim. Acta 288, 68–82. https://doi.org/10.1016/j.gca.2020.07.043.

Voegelin, A.R., Pettke, T., Greber, N.D., von Niederhäusern, B., Nägler, T.F., 2014. Magma differentiation fractionates Mo isotope ratios: evidence from the Kos Plateau Tuff (Aegean Arc). Lithos 190–191, 440–448. https://doi.org/10.1016/j.lithos.2013.12.016.

Waters, L.E., Cottrell, E., Coombs, M.L., Kelley, K.A., 2021. Generation of Calc-Alkaline magmas during crystallization at high oxygen fugacity: an experimental and petrologic study of Tephras from Buldir Volcano, Western Aleutian arc, Alaska, USA. J. Petrol. 62 (3), egaa104. https://doi.org/10.1093/petrology/egaa104.

Werner, R., Hoernle, K., Hauff, F., Portnyagin, M., Yogodzinski, G., Ziegler, A., 2016. RV Sonne Fahrtbericht / Cruise Report SO249 Bering – Origin and Evolution of the Bering Sea: an Integrated Geochronological, Volcanological, Petrological and Geochemical Approach, Leg 1: Dutch Harbor (U.S.A.) – Petropavlovsk-Kamchatsky (Russia), 05.06.2016–15.07.2016, Leg 2: Petropavlovsk-Kamchatsky (Russia) – Tomakomai (Japan), 16.07.2016–14.08.2016. GEOMAR Report 30. GEOMAR Helmholtz-Zentrum für Ozeanforschung, Kiel, Germany. 451 pp.

Willbold, M., Hibbert, K., Lai, Y.-J., Freymuth, H., Hin, R.C., Coath, C., Vils, F., Elliott, T., 2016. High-precision mass-dependent molybdenum isotope variations in magmatic rocks determined by double-spike MC-ICP-MS. Geostand. Geoanal. Res. 40 (3), 389–403. https://doi.org/10.1111/ggr.12109.

Wille, M., Nebel, O., Pettke, T., Vroon, P.Z., König, S., Schoenberg, R., 2018. Molybdenum isotope variations in calc-alkaline lavas from the Banda arc, Indonesia: assessing the effect of crystal fractionation in creating isotopically heavy continental crust. Chem. Geol. 485, 1–13. https://doi.org/10.1016/j.chemgeo.2018.02.037.

Yang, J., Siebert, C., Barling, J., Savage, P., Liang, Y.-H., Halliday, A.N., 2015. Absence of molybdenum isotope fractionation during magmatic differentiation at Hekla volcano, Iceland. Geochim. Cosmochim. Acta 162, 126–136. https://doi.org/10.1016/j.gca.2015.04.011.

Yogodzinski, G.M., Brown, S.T., Kelemen, P.B., Vervoort, J.D., Portnyagin, M., Sims, K.W.W., Hoernle, K., Jicha, B.R., Werner, R., 2015. The role of subducted basalt in the source of island arc magmas: evidence from seafloor lavas of the Western Aleutians. J. Petrol. 56 (3), 441–492. https://doi.org/10.1093/petrology/egv006.

Yogodzinski, G.M., Kelemen, P.B., Hoernle, K., Brown, S.T., Bindeman, I., Vervoort, J.D., Sims, K.W.W., Portnyagin, M., Werner, R., 2017. Sr and O isotopes in western Aleutian seafloor lavas: implications for the source of fluids and trace element character of arc volcanic rocks. Earth Planet. Sci. Lett. 475, 169–180. https://doi.org/10.1016/j.epsl.2017.07.007.

Yogodzinski, G.M., Vervoort, J.D., Brown, S.T., Gerseny, M., 2010. Subduction controls of Hf and Nd isotopes in lavas of the Aleutian island arc. Earth Planet. Sci. Lett. 300 (3–4), 226–238. https://doi.org/10.1016/j.epsl.2010.09.035.

Zack, T., Kronz, A., Foley, S.F., Rivers, T., 2002. Trace element abundances in rutiles from eclogites and associated garnet mica schists. Chem. Geol. 184 (1–2), 97–122. https://doi.org/10.1016/S0009-2541(01)00357-6.

Zimmer, M.M., Plank, T., Hauri, E.H., Yogodzinski, G.M., Stelling, P., Larsen, J., Singer, B., Jicha, B., Mandeville, C., Nye, C.J., 2010. The role of water in generating the calc-alkaline trend: new volatile data for Aleutian magmas and a New Tholeiitic index. J. Petrol. 51 (12), 2411–2444. https://doi.org/10.1093/petrology/egq062.